Biomaterials 33 (2012) 402–411

Contents lists available at SciVerse ScienceDirect

Biomaterials

journal homepage: www.elsevier.com/locate/biomaterials

The triggering of apoptosis in macrophages by pristine graphene through the MAPK and TGF-beta signaling pathways

Yang Li [a,b,1], Ying Liu [a,1], Yujian Fu [a,b], Taotao Wei [c], Laurent Le Guyader [a], Ge Gao [a], Ru-Shi Liu [d,e,**], Yan-Zhong Chang [b,***], Chunying Chen [a,*]

[a] CAS Key Lab for Biomedical Effects of Nanomaterials and Nanosafety, National Center for Nanoscience and Technology of China, Chinese Academy of Sciences, No. 11, Beiyitiao, Zhongguancun, Beijing 100190, PR China
[b] Laboratory of Molecular Iron Metabolism, College of Life Science, Hebei Normal University, Shijiazhuang 050016, PR China
[c] National Laboratory of Biomacromolecules, Institute of Biophysics, Chinese Academy of Sciences, Beijing 100101, PR China
[d] Department of Chemistry, National Taiwan University, Taipei 106, Taiwan
[e] Genomics Research Center, Academia Sinica, Taipei 115, Taiwan

ARTICLE INFO

Article history:
Received 20 August 2011
Accepted 29 September 2011
Available online 22 October 2011

Keywords:
Graphene
Apoptosis
Macrophage
Mitogen activated protein kinase
TGF-beta

ABSTRACT

With the development of nanotechnology and the wide use of graphene, it has become necessary to assess the potential biological adverse effects of graphene. However, most of the recent publications are focused on various modified graphenes. We demonstrated biological effects of commercial pristine graphene in murine RAW 264.7 macrophages, which is an important effector cells of the innate immune system. We found that the pristine graphene can induce cytotoxicity through the depletion of the mitochondrial membrane potential (MMP) and the increase of intracellular reactive oxygen species (ROS), then trigger apoptosis by activation of the mitochondrial pathway. The MAPKs (JNK, ERK and p38) as well as the TGF-beta-related signaling pathways were found to be activated in the pristine graphene-treated cells, which activated Bim and Bax, two pro-apoptotic member of Bcl-2 protein family. Consequently, the caspase 3 and its downstream effector proteins such as PARP were activated and the execution of apoptosis was initiated. This study provides an insight for the suppression of the apoptosis induced by the graphene through the mitochondrial pathways, the MAPKs- and TGF-beta-related signaling pathways.

1. Introduction

Recently, nanotechnologies have undergone a rapid growth all over the world, with the apparition of a broad array of nanomaterials which will more and more affect our life since incorporated in many daily-used products. Among these new materials one can cite nano-ceramics, nano-polymers, metals and alloys, biological nano-materials and of course carbon-based nanomaterials like graphene [1–3]. Graphene is a single-atom-thick sheet of sp^2-bonded carbon atoms in a closely packed honeycomb two-dimensional lattice, and as one of the most fascinating nanomaterial has drawn a lot of attention because of its unique physicochemical properties. This promising material can be qualified for condensed-matter and high-energy physics [4–6], material science [7–9], cellular imaging [10] drug delivery and biological material applications [11–17] and a wide range of other technological applications [18–22], such as bioelectronics and biosensing [23,24].

Many studies have shown that nanoparticles (NPs) can have adverse effects on health [25–28], which are mainly due to their smaller size, larger surface area per mass and more reactive properties [29,30]. Some modified nanomaterials such as fullerenes, carbon nanotubes, iron oxide particles can be quickly endocytosed and exert certain cellular response [28,31]. Because of the large-scale production of graphene and its derivatives to reach the industry's increasing needs and consequently with graphene being potentially in contact to the environment, we should consider the environmental issue and the safety of these nanomaterials, no matter how this materials benefit to our daily life. However there is no much information concerning the newly developed graphene, with only a limited number of reports available. Yang et al. [32] have proven that functional graphene could be metabolized out of the body and did not induce appreciable toxicity during the three

* Corresponding author. Tel.: +86 10 82545560; fax: +86 10 62656765.
** Corresponding author. Department of Chemistry, National Taiwan University, Taiwan.
*** Corresponding author.
E-mail addresses: rsliu@ntu.edu.tw (R.S. Liu), chang7676@163.com (Y.-Z. Chang), chenchy@nanoctr.cn (C. Chen).
[1] Yang Li and Ying Liu contributed equally to this work.

0142-9612/$ – see front matter © 2011 Elsevier Ltd. All rights reserved.
doi:10.1016/j.biomaterials.2011.09.091

months of blood biochemistry tests, hematological analyses and histological examinations. Chang et al. [33] used graphene oxide to assess toxicity *in vitro* and proved that this material could not induce apparent cell death despite obvious intracellular oxidative stress. However, some other studies on this material obtained different results [34,35]. Considering that most studies have used modified graphene and have only focused on basic phenomena without deeply explaining the mechanisms underlying its toxicity, we still need to investigate the safety issue of pristine graphene systematically, and the underlying mechanisms shoud be explored. In an attempt to address these questions, we used pristine graphene instead of modified graphene to evaluate its toxicity *in vitro* in the present investigation. Murine macrophage-like RAW 264.7 cells was used as the cell model, since macrophages, the important member of the innate immune system, are targets of several nanomaterials.

Mitochondria are centers for energy generation in cells and are also involved in various cell signal pathways. Mitochondria can act as a major checkpoint of apoptotic regulation. They serve as sensors and amplifiers of cellular damage. Following mitochondrial outer membrane permeabilization (MOMP), mitochondria release a number of factors such as cytochrome c, Smac/DIABLO, AIF (apoptosis inducing factor) and endonuclease G, which are critically involved in cell death signaling. Mitochondria are also centrally involved in the activation of caspases, a family of otherwise dormant cysteine proteases that cleave a subset of cellular proteins. Considering that studies on nanomaterials have shown that NPs can cause cell cytotoxicity by induce the dysfunction of mitochondria [3,28,36] and initiate the consequent accumulation of intracellular reactive oxygen species (ROS), we focused on the effects of pristine graphene on the mitochondria to explore the pathways involved in the modulation of cells by pristine graphene. Therefore, in this work, the cytotoxicity of pristine graphene was evaluated and its effects on mitochondrial membrane potential (MMP), intracellular ROS and apoptosis were further studied. The influences of graphene treatment on the MAPKs (JNK, ERK and p38) as well as the TGF-beta-related signaling pathways were finally investigated by using Western-Blotting and quantitative real-time PCR.

2. Materials and methods

2.1. Characterization of pristine graphene

The commercial graphene sample (pristine graphene) was obtained from the Kinik Company (Taiwan). Scanning electron microscope (Hitachi S4800 + EDS) was used to characterize the prisitin graphene. Sample were prepare in aqueous solution then vortexed for 1 min and sonicated (KQ 500-DE) for 3 h. At last prepared samples were observed in an accelerating voltage of 5 kV. Graphite and pristine graphene (the commercial sample) are identified using an X-ray diffractometer (XRD, PANalytical PW3040/60 X′ Pert pro) with a copper target ($\lambda = 1.541$ Å) that is excited at 45 kV and 40 mA. Raman spectrum is collected on a Jobin Yvon LabRam 300 system using a 632.8 nm He–Ne laser with its intensity of 6 mW. The pixel resolution is about 3 cm^{-1}, whereas the peak resolution is about 15 cm^{-1} for the Silicon wafer.

2.2. Dispersion of graphene and preparation of stock solutions

A 250 μg/mL pristine graphene suspension was prepared with 1% pluronic F108 (Sigma–Aldrich, batch#:09308BJ). The obtained Graphene suspension was vortexed for 1 min and sonicated (KQ 500-DE) for 30 min. About 30 μL suspension was taken out and deposited on a fresh mica surface, and then the mica was measured by Atomic Force Microscopy (AFM, Agilent 5500 Agilent Co.). Before biological test, the graphene suspension was sonicated for 5 additional minutes, and then added to the medium to disperse the Graphene at concentrations of 5, 10, 20, 40, 80 and 100 μg/mL.

2.3. Cytotoxicity assay

The cytotoxicity assay, involving the reduction of a water-soluble tetrazolium salt, was performed using a Cell Counting Kit-8 (Dojindo Laboratories, Japan) according to the instructions of the manufacturer. 100μL of a cell suspension (10000 cells/well) was seeded into a 96-well plate and put in a humidified incubator for 24 h (37 °C, 5% CO_2). Then the medium was replaced by fresh medium (control) or graphene-containing media at different concentrations. After 48 h, the culture supernatant was removed and the cells were washed 3 times with PBS (pH 7.4). Then a 1:10 mixture of the tetrazolium reagent (from the Cell Counting Kit-8) and medium was added into the cell flask. After incubation at 37 °C for 2 h, the absorbance was measured at 450 nm using a TECAN Infinite M200 microplate reader (Tecan, Durham, USA; Detection: 450 nm, reference: 650 nm) to test the cell viability. Each experiment was repeated independently three times.

2.4. Measurement of intracellular ROS

A cell suspension (density $4 \cdot 10^5$/mL) was dispersed in a 6-well plate for flow cytometry. The cells were pre-incubated for 24 h in a humidified incubator (37 °C, 5% CO_2). Then the medium was replaced with fresh medium (control) or graphene-containing media at different concentrations for 24 or 48 h. Cells were washed three times with PBS and incubated with 10 μM CM_H2 DCFDA for 30 min. Then the cells were washed three times with PBS to eliminate the excess of unreacted DCFDA. Finally flow cytometry (Beckman Coulter, USA, 488 nm, FL1) was used to measure the fluorescence of the intracellular reduced DCFDA molecules, which is directly related to the intracellular ROS level.

2.5. MMP assay

The JC-1 dye (5,50,6,60-tetrachloro-1,10,3,30-tetraethylbenzimidazolocarbocyanine iodide, a potential-dependent J-aggregate forming delocalized lipophilic cation) was used to determine the reduction of mitochondrial membrane potential. Briefly, stock solution of 1.0 mg/mL JC-1 (Molecular Probes, Invitrogen, USA) was prepared in DMSO and stored at −20 °C shortly before use. RAW 264.7 cells were cultured on glass coverslips for laser confocal scanning microscope in a humidified incubator (at 37 °C, 5% CO2). After 12 h the medium was replaced with fresh medium or media containing pristine graphene at different concentrations. After incubation for 12 or 24 h, cells were washed 3 times with PBS and the JC-1 (1 μg/mL) dye was added into each well. After incubation for 20 min, cells were washed 3 times with PBS. Cells were then imaged with a laser confocal scanning microscope (Olympus FV 500).

2.6. Measurement of apoptosis and necrosis

RAW 264.7 cells were pre-incubated for 12 h in a humidified incubator (37 °C, 5% CO_2). Then the medium was replaced with fresh graphene-containing media at different concentrations for 24 and 48 h. Cells were washed three times with PBS and harvested. Then the double-stained annexin V-FITC Kit (BENDER, containing annexin V-FITC and propidium iodide (PI)) was used to incubate the cells which were analyzed using a Cell Lab Quanta SC flow cytometry (Beckman Coulter, USA, 488 nm, FL1).

2.7. Cellular ultrastructure observation by transmission electron microscopy

The ultrastructural alterations of RAW 264.7 cells induced by pristine graphene were observed with a Hitachi TEM (Hitachi H-600, Japan) at an accelerating voltage of 100 kV. After a 48-h exposure, cells were harvested and washed with PBS and prefixed with 2.5% glutaraldehyde at 4 °C for 3 h.

2.8. Western-blotting

RAW 264.7 cells, grown to 70% confluence in a flask, were cultured with a medium containing 20 μg/mL pristine graphene. After 48 h, cells were washed with PBS, harvested with a scraper and centrifuged at 2000 × g for 10 min at 4 °C. After discarding the supernatant, cells were lysed to collect the cellular proteins. Equal amounts (50 μg) of proteins were separated on 12% SDS-PAGE gels and transferred to nitrocellulose membranes. The membranes were blocked with 5% non-fat milk in TBST at room temperature. The primary antibody was used at 1:1000 dilution and the secondary antibody was used at 1:5000 dilution (information on antibodies can be find in the supporting information section). Blots were developed using enhanced chemiluminescence. The tested proteins were Phospho-p38 MAPKinase (P-p38), p38 MAPKinase (p38), Phospho-JNK (P-JNK), JNK, Phospho-ERK (P-ERK), ERK, Phospho-Smad2, Smad2, Bim, Bax, caspase 3, Bcl-2, PARP and β-actin.

2.9. Total RNA isolation and analysis by quantitative real-time PCR

RAW 264.7 cells, grown to 70% confluence in a flask, were cultured with the medium containing 20 μg/mL graphene. After 48 h, cells were washed 3 times with PBS and 1 mL of Trizol Reagent was added to each flask. Samples were transferred to a Phase Lock tube and incubated at room temperature for 5 min. Then 200 μL of chloroform was added (per 1 mL Trizol) and samples were shaked vigorously (not vortexed) for 15 s to mix well, incubated at room temperature for 15 min and centrifuged at 12,000 × g for 15 min at 4 °C to separate the different phases. The upper (clear) aqueous layer of each sample was transferred into a fresh tube

containing 0.5 mL of isopropanol and mixed thoroughly by shaking for 15 s and incubated at room temperature for 10 min. Samples were again centrifuged at 11,000 × g at 4 °C for 10–30 min to pellet the RNA. The supernatant was carefully removed and 1 mL of 75% DEPC-ethanol was added to each tube then gently vortexed for 10 s to wash the pellet. The RNA was re-pelleted by centrifugation at 8000 × g at 4 °C for 5 min, then dissolved in DEPC-dH_2O (30–100 μL, depending on the desired yield) by gentle pipetting. The purity was determined from the absorbance ratio (A260/A280) (at or above 1.80, to 2.00 OD). RNA samples were then reverse transcribed to cDNA using Oligo dT (Promega). The resulting cDNA samples were analyzed by quantitative real-time PCR using (Eppendorf), using SYBR green as fluorescence dye, as described previously. Relative quantifications of mRNA expression in the genes of interest were calculated using the comparative threshold cycle number for each sample. The following genes were measured: TNF-alpha, TGF-beta, TGF-beta receptor I, TGF-beta receptor II, Smad2, Smad3, Smad4, Smad7, beta-Actin. The primer sequences are list in supporting table 2.

3. Results and discussion

3.1. Characterization of pristine graphene

Pristine graphene was analyzed by SEM for characterization. In Fig. 1A, we can clearly observe the feature of graphene, with some of the sheets in the small scale and some other in the large scale. Based on the scanning electron microscope and energy dispersive spectrometry, therefore there is trace amount of metal impurity in this commercial graphene. The corresponding XRD patterns are plotted in Fig. 1B. As indicated, the broaden C (002) peak for graphene was observed, which is shifted to $2\theta = 25.67$. The layer to layer distance for graphene is increased from 0.335 nm to 0.347 nm as compared to the pristine graphite. Fig. 1C shows the Raman spectrum of graphene (the commercial sample). Two featured peaks associated with the D-band and the G-band causing by the disorder of the graphite edges and the in-phase vibration of the graphite lattice are clearly appeared. Due to the formation of individual graphene nanosheets, more disordered structure is exhibited, resulting in the higher I_D/I_G (~1.23). The size and morphology of the graphene in surfactant of 1% pluronic F108 is given in Fig. 1D with thickness of 2–3 nm and size of around 500–1000 nm, and the dots in the AFM image are pluronic F108.

3.2. The cytotoxicity of pristine graphene

To assess the overall cytotoxic effects of pristine graphene on cells, we investigated the viability of RAW 264.7 macrophages incubated with different concentrations of pristine graphene for 48 h. As shown in Fig. 1E, low concentrations (i.e. 20 μg/mL) of pristine graphene-induced slight cell death in RAW 264.7 cells, with more than 80% of the cells remain unaffected. However the highest concentration (100 μg/mL) of pristine graphene-induced significant cytotoxicity, with about 78% of the cells dead. These data reveal that pristine graphene shows an obvious dose-dependent cytotoxic effect, which is in accordance with other nanomaterials [34]. How could pristine graphene influences the intracellular events that are important for the fate of cells, and what are the fine mechanisms of this cytotoxicity? Those are the questions we are going to address below.

3.3. ROS production induced by pristine graphene

Generally when cells were exposed to nanomaterials, an increase in the intracellular reactive oxygen species (ROS) level could be provoked. Accumulation of intracellular ROS is the main characteristic of the oxidative stress, so the detection of ROS generation reflects the intracellular oxidative stress status, which is an important indicator of the cell health. It has been well

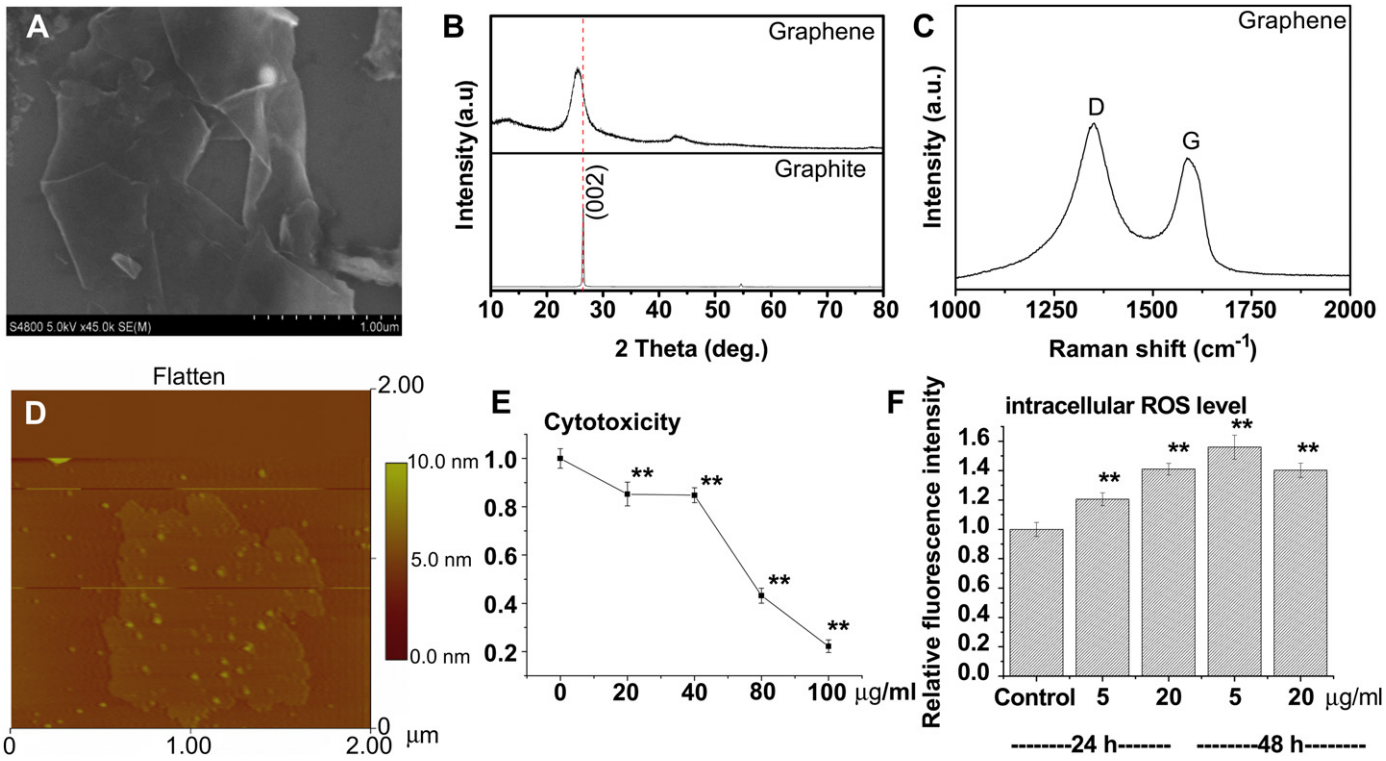

Fig. 1. The characteristics of pristine graphene and its toxicity in RAW 264.7 macrophage cells. A) The SEM image of pristine graphene; B) XRD patterns of pristine graphene and graphite; C) Raman spectrum of pristine graphene; D) The AFM image of the graphene in 1% pluronic F108; E) The cell viability of RAW 264.7 cells incubated with culture medium containing pristine graphene at 20, 40, 80 or 100 μg/mL for 48 h; F) The intracellular ROS levels of cells incubated with culture medium containing pristine graphene at 5 or 20 μg/mL for 24 or 48 h (**$P < 0.01$, compared to control).

documented that ROS can induce intracellular protein inactivation (through oxidation and nitration), lipid peroxidation, dysfunction of the mitochondria and eventually apoptosis or necrosis [36–38]. In the present investigation we measured the intracellular ROS level in RAW 264.7 cells after incubation with pristine graphene for 24 or 48 h. Fig. 1F showed that pristine graphene exposure induced intracellular ROS generation in a time- and dose-dependent manner, which is in accordance with a previous study with modified graphene from Chang's group [33]. The highest ROS level was found in RAW 264.7 cells exposed to a dose of 5 μg/mL of pristine graphene for 48 h. More importantly, we found that the ROS level is correlated to the rate of cell death measured in Fig. 1E. Then we tried to explore the underlying mechanism of ROS-related cell death in pristine graphene-treated cells.

3.4. The alteration of mitochondrial membrane potential

The depolarization of the mitochondrial membranes is one of the key events associated with the accumulation of intracellular ROS, so we determined the depolarization of mitochondria in pristine grapheme-treated RAW 264.7 cells by measuring the alteration of mitochondrial membrane potential (MMP). The MMP plays a key role in maintaining the proton gradient across the mitochondrial membrane and is essential for the electron transfer chain. In depolarized mitochondrion, the mitochondrial membrane potential was lost due to the alteration of the mitochondrial membrane integrity. Disruptions of the MMP may cause severe consequences problems, including decrease in ATP synthesis, increase in ROS generation, and the redistribution of pro-apoptotic mitochondrial factors [39,40]. In normal cells, due to the electrochemical potential gradient, the dye concentrates in the mitochondrial matrix, where it forms red fluorescent aggregates (J-aggregates). In apoptotic cells, the dye stays in the cytoplasm as monomers and fluoresces green, therefore, JC-1 is particularly useful for apoptosis studies. The results, presented in Fig. 2, show that the cells incubated with pristine graphene exhibit obvious substantial dose-dependent MMP decrease compared to the control, suggesting the occurring of mitochondrial membrane depolarization. Moreover, the decrease in mitochondrial MMP also present a time-dependence as we find the MMP decrease in cells treated with pristine graphene for 24 h is stronger than cells treated for 12 h. Both the decrease in mitochondrial MMP and the accumulation of cellular ROS are hallmarks of mitochondria-related apoptosis. Indeed, if the mitochondrial damage is significant, a cascade process characterized by the permeabilization of mitochondrial outer membrane will occur, and pro-apoptotic molecules will be relocated from the mitochondria to the cytoplasm. This is recognized as "the point of no return" [41]. Once this cascade process is initiated, the pro-apoptotic machinery will be activated and causes the execution of apoptosis [42]. Our next experiment aimed to address whether the mitochondria pathway are involved in pristine grapheme-treated cells.

3.5. Apoptosis caused by pristine graphene

Since we have demonstrated that pristine graphene could induce the increase in intracellular ROS, the depolarization of mitochondria, and the decrease in cell viability in RAW 264.7 cells, we then quantified the percentage of cells in early apoptotic, apoptototic or late apoptotic (necrotic) stages in RAW 264.7 cells exposed different concentrations of pristine graphene for different time, by flow cytometry. From Fig. 3A, we can conclude that exposure of cells to pristine graphene caused an increase in the proportion of apoptosis and necrosis as a function of the incubation time. Moreover, the highest dose (50 μg/mL) induced the highest fraction of late apoptotic (necrotic) cells, regardless the incubation time.

The pristine graphene-induced apoptosis in RAW 264.7 cells was further confirmed by morphological criteria. Fig. 3B shows the typical TEM ultrastructural images of untreated cells (left) or cells exposed for 48 h to pristine graphene (middle and right). Large phagocytic vesicles were observed in pristine graphene-treated cells, suggesting that pristine graphene could be translocated into the murine macrophage-like RAW 264.7 cells via phagocytosis and need further confirmation by other techniques such as Raman measurement. More importantly, typical apoptotic cells could be observed in pristine graphene-treated cells (right).

Apoptosis is a coordinated process that can be triggered through two different pathways, the death-receptor pathway (triggered by members of the death-receptor superfamily) and the mitochondrial pathway (in response to extracellular cues and internal DNA damage) [43]. Since the pristine grapheme-induced apoptosis is accompanied by the loss of mitochondrial MMP and the increase in cellular ROS level, we think the mitochondrial pathway might be the dominant mechanism underlying pristine graphene-induced apoptosis. We assumed that pristine graphene altered the mitochondrial integrity via an mechanism related with the activation of the pro-apopototic member of Bcl-2 family and the MAPK cascades

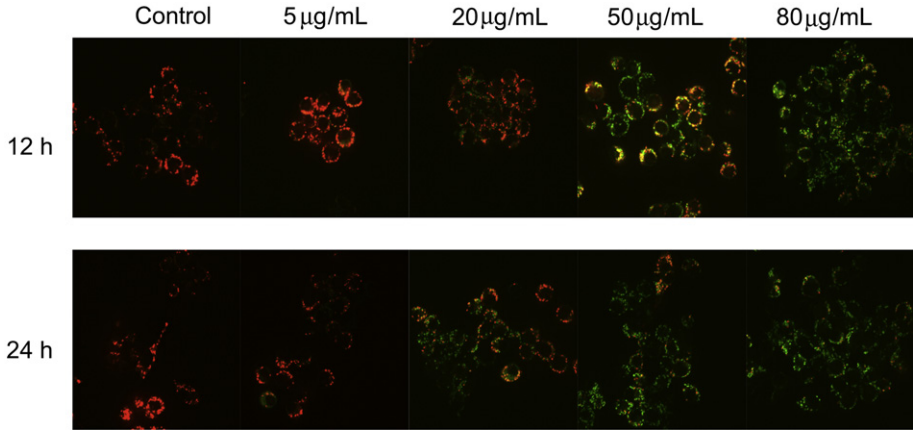

Fig. 2. The variation of mitochondrial membrane potential of RAW 264.7 cells incubated with culture medium containing pristine graphene at 5, 20, 50, 80 μg/mL for 12 or 24 h. The mitochondrion-specific dye JC-1 was used to detect changes in mitochondrial membrane potential. The monomer JC-1 has green fluorescence (527 nm), while the J-aggregates have red fluorescence (590 nm). Apoptotic cells mainly show green fluorescence, while healthy cells show red and green fluorescence (yellow when merged) making JC-1 suitable for the detection of mitochondrial damage. (For interpretation of the references to colour in this figure legend, the reader is referred to the web version of this article.)

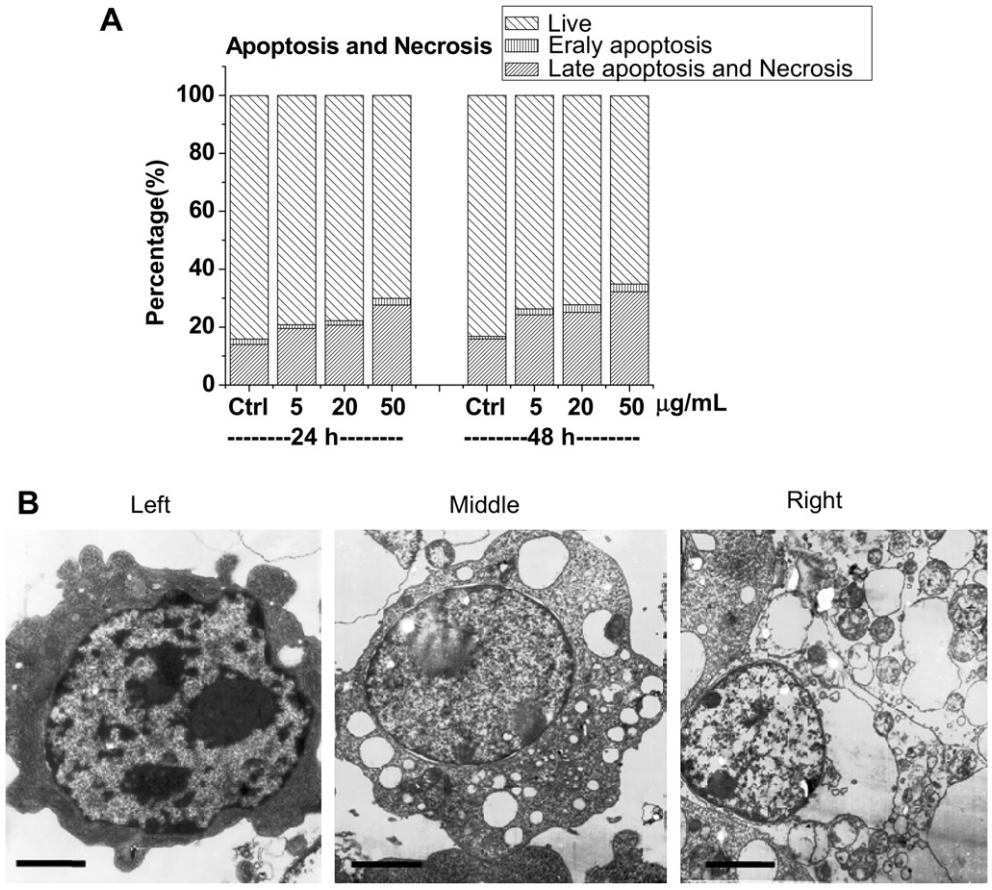

Fig. 3. The apoptosis and necrosis of RAW 264.7 cells incubated with pristine graphene. A) The ratio of apoptosis and necrosis of cells incubated in culture medium containing pristine graphene at 5, 20 or 50 μg/mL for 24 or 48 h; B) The TEM images of cells incubated with 20 μg/mL graphene for 48 h, Left: Control, Middle and Right, Graphene exposure. Bar, 2 μm for Left and Middle images, and 1 μm for Right image.

[44]. To demonstrate this mechanism, we further investigated some potentially triggered signal pathways.

3.6. Activation of MAPK signal pathways

During apoptosis, a broad array of cell signal pathways are activated, and numerous genes and proteins are involved. ROS are closely related with the apoptosis and the proliferation of cells, via the activation of mitogen-activated protein kinase (MAPK) cascades. MAPKs are regarded as stress-sensitive kinases and are involved in apoptotic cell death [45] in oxidative stressed cells.

The MAPKs regulate essential cellular events including the proliferation, differentiation or apoptosis. The MAPKs signal pathway includes the extracellular signal-regulated kinase (ERK, components of the MAPK cascades), the p38 mitogen-activated protein kinases (p38) and c-Jun N-terminal kinase (JNK) signal pathways. The MAPKs can even be stimulated by UV or H_2O_2 and then induce cell apoptosis [46,47]. Thus it is reasonable to assume that the ROS generation and mitochondrial damage induced by pristine graphene can provoke MAPKs signal pathway.

In order to determine the potential signal pathways involved, we measured the contents of ERK, p38 and JNK protein (and their phosphorylated form) in RAW 264.7 cells exposed to 20 μg/mL pristine graphene for 48 h. Fig. 4A shown that the content of total ERK, JNK and p38 protein kinase were similar before and after the pristine graphene exposure. However the level of the corresponding phosphorylated kinases was significantly higher in all cases, meaning that all the three MAPKs signal pathways were activated upon pristine graphene treatment. Moreover, the highest difference in between non activated and activated (phosphorylated) pool of kinases was found for JNK. This makes sense since the JNK pathway is typically activated by external "death" stimuli, like TNF-alpha, to trigger the mitochondrial apoptotic pathway [48]. The p38 protein activated by ROS can also induce cell apoptosis following a stimulation by TNF-alpha and recruit caspase-8 and caspase-3 [49]. In addition the activation of ERK pathway can also induce apoptosis, as shown by recent works [50–53]. Therefore we confirmed that the recruited MAPKs must be the potential proteins inducing cell apoptosis.

Apoptosis signal-regulating kinase 1 (ASK1) is an evolutionary conserved mitogen-activated protein 3-kinase that activates both JNK and p38 MAPK, which may also be triggered by ROS [54,55]. ASK1-induced and ROS-dependent activation of MAPKs is crucial for the apoptosis [56]. In the case of oxidative stress, a positive feedback may occur in the ASK1-p38-TNF-alpha pathway, which enhances ROS-mediated apoptosis. ASK1 activates both JNK and p38 MAPK, then the activated p38 translocate into the nucleus to stimulate the expression of MK2. After exiting from the nucleus, MK2 increases the TNF-alpha production. On the other hand, enhanced TNF-alpha and ROS activate ASK1 activity [55], which leads to the activation of JNK. In order to demonstrate the existence of this positive apoptosis feedback, we measured the TNF-alpha intracellular mRNA level in cells exposed or not to pristine graphene (Fig. 4B). As expected, the results clearly showed a 5-fold increase in TNF-alpha mRNA level in the treated cells compared to the control cells.

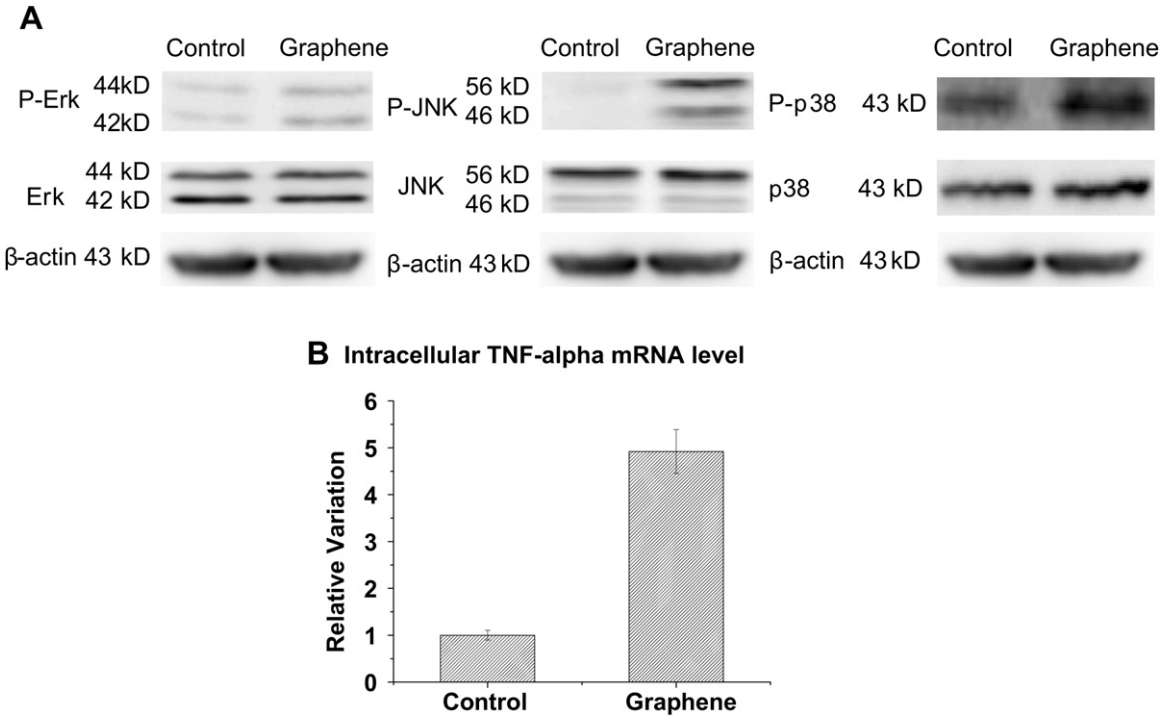

Fig. 4. Effects of pristine graphene on the MAPK apoptotic pathway. Protein expressions and mRNA variations were assessed. Western blot and real-time PCR in RAW 264.7 cells incubated with 20 μg/mL pristine graphene for 48 h. A) The expression levels of MAPKs proteins in parallel with β-actin expression as a loading control. Pristine graphene significantly increase phosphor-JNK (P-JNK), phosphor-Erk (P-Erk) and phosphor-p38 (P-p38). Total protein of JNK and Erk expression were unaltered, but a littler increase of p38. B) Effects of pristine graphene on the TNF-alpha mRNA level. A significantly increase of the mRNA levels of TNF-alpha after incubated with pristine graphene.

3.7. Activation of TGF-beta signal pathway

As we mentioned above, the apoptotic cell death is a complicated process involving the expression of many genes and the activation of different signaling pathways, and has its own diversity. The transforming growth factor-beta (TGF-beta) has been shown to play a key role in cell apoptosis in various cell lines [57,58], especially in immune-related cells. In addition, many studies have investigated the downstream proteins of TGF-beta —the Smad protein family— suggesting that Smads have tremendous regulative functions in cell apoptosis. For instance, Patil et al. found that the inhibition of the Smads signaling pathway can be an obstacle to the apoptosis by TGF-beta [59]. In order to verify this fact in our system, both the TGF-beta and Smads signaling pathways were investigated by assessing the mRNA levels of various proteins by quantitative real-time PCR in treated (20 μg/mL of pristine graphene for 48 h) and control RAW macrophages (Fig. 5). Macrophages incubated with pristine graphene exhibited an increased TGF-beta mRNA level (Fig. 5A). The mRNA of the TGF-beta receptors I and II, which connect the extracellular TGF-beta signal and the intracellular effectors, also undergone a tremendous increase (Fig. 5B), and this further proved the important role played by the TGF-beta pathway in response to pristine graphene exposure. We therefore proceeded to the next step which consisted on the evaluation of the Smads signaling pathway involvement. The Fig. 5C revealed that the R-Smads (Smad2/3) and Co-Smad (Smad4) mRNA levels significantly increased, showing a stimulated transcription activity. The Fig. 5E shows that the phosphorylation of R-Smad has occurred. All these results demonstrated that pristine graphene stimulated and activated the TGF-beta and Smads signaling pathway which trigger the apoptosis. We also determined the expression level of Inhibitor-Smad (Smad7) and found a 3-fold increase in the mRNA level compared to the control (Fig. 5D). Smad7 is a well known inhibitor of the Smads but is has also been reported to enhance the TGF-beta, and even the TNF-alpha-mediated apoptosis in some cell lines [60], which could be the case in the present study.

3.8. Crosstalk within the mitochondrial apoptotic pathway

As we reported previous, the signaling pathways represent an intricate and highly regulated system, with positive and negative feedbacks in cells. Some publications have demonstrate that the ERK protein can recruit the Smads proteins [61], then Smads must play a key role in the apoptosis. Some other researches has proven that the TGF-beta pathway can activate the MAPKs and induce the apoptosis [62]. So there is a quite a number of candidate proteins that can be recruited for this purpose.

Bim, a pro-apoptotic member of the Bcl-2 family, can be activated by either Smads proteins or JNK. Activated Bim recruit the Bax protein, another pro-apoptotic member protein of the Bcl-2 family, to induce the permeabilization of mitochondrial outer membrane, and cause the relocation of mitochondrial pro-apoptotic factors into the cytosol, where these factors activates the cascade of caspases, and finally caused the activation of caspase-3. Caspase-3 is the important evectional caspase of the apoptosis [63]. To address the possible involvement of these pathway in pristine graphene-induced apoptosis, the expression of Bim and Bax were assessed by western blot in treated (48-h exposure of 20 μg/mL of pristine graphene) and control cells (Fig. 6A). The marked increase in Bim and Bax protein levels after exposure to pristine graphene were another evidence of a TGF-beta and MAPKs combined role in mitochondria-mediated apoptosis.

Generally, caspase-3 is activated in apoptotic cells by both extrinsic (death ligand) and intrinsic (mitochondrial) pathways [64–66] and is regarded as one of the most important executional

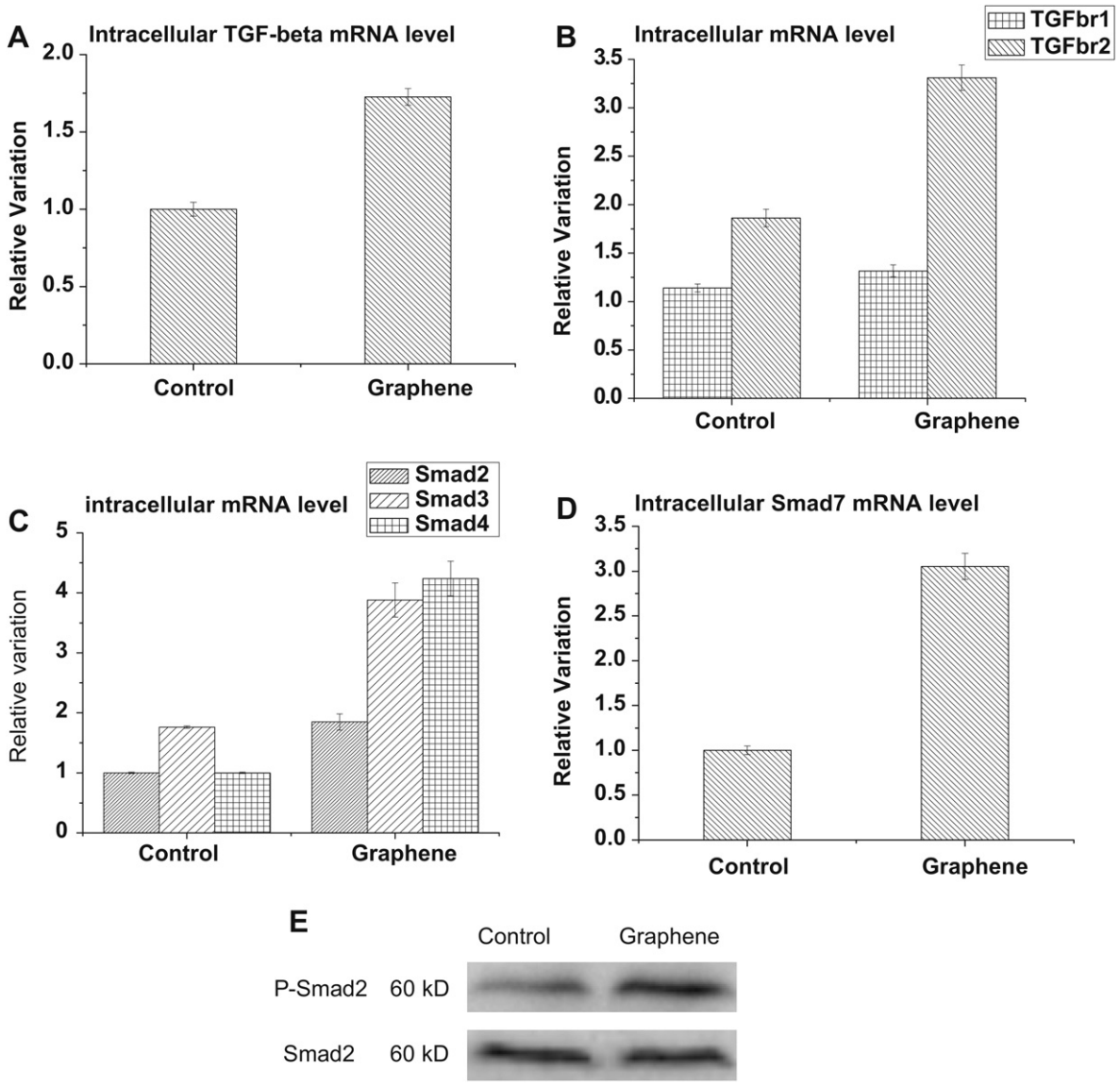

Fig. 5. Effects of pristine graphene on the TGF-beta pathway of RAW 264.7 cells. Protein expressions and mRNA variations were assessed. Western blot and real-time PCR of the TGF-beta signaling pathway variations of RAW 264.7 cells incubated with 20 μg/mL pristine graphene for 48 h (*$P < 0.05$) A) Pristine graphene increase the TGF-beta mRNA level; B) Effects of pristine graphene on TGF-beta receptor 1/2 mRNA level. Pristine graphene significantly increase the TGF-beta receptor 2, but do not have to much effect on TGF-beta receptor 1; C) Pristine graphene can significantly increase the Smad2/3/4 mRNA level; D) Pristine graphene can significantly increase the Smad7 mRNA level; E) Effects of pristine graphene on Smad2 and P-Smad2 protein variations. Pristine graphene can significantly increase the phosphor-Smad2 (P-Smad2). But total protein (Smad2) expression was unaltered.

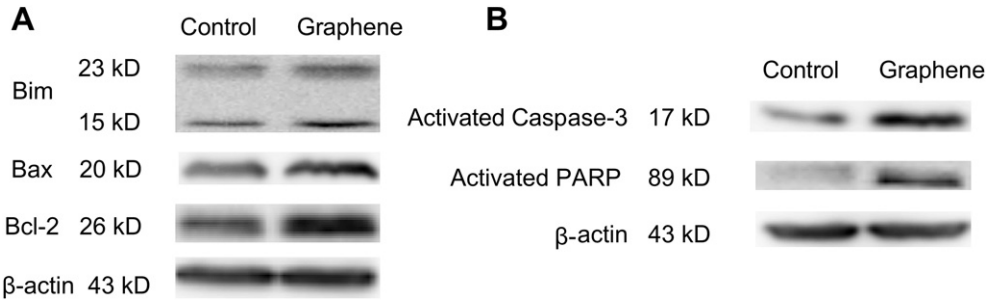

Fig. 6. Effects of pristine graphene on Bcl-2 super families and apoptosis key proteins of RAW 264.7 cells. Western blot were used for RAW 264.7 cells incubated with 20 μg/mL of pristine graphene for 48 h. A) The protein level variations of Bcl-2 super families after incubated with pristine graphene. The Bim was increase a little, but significantly increase with Bax and Bcl-2; B) Effect of pristine graphene activated caspase-3 and PARP. Both active caspase-3 and active PARP have significantly increase after incubated with pristine graphene.

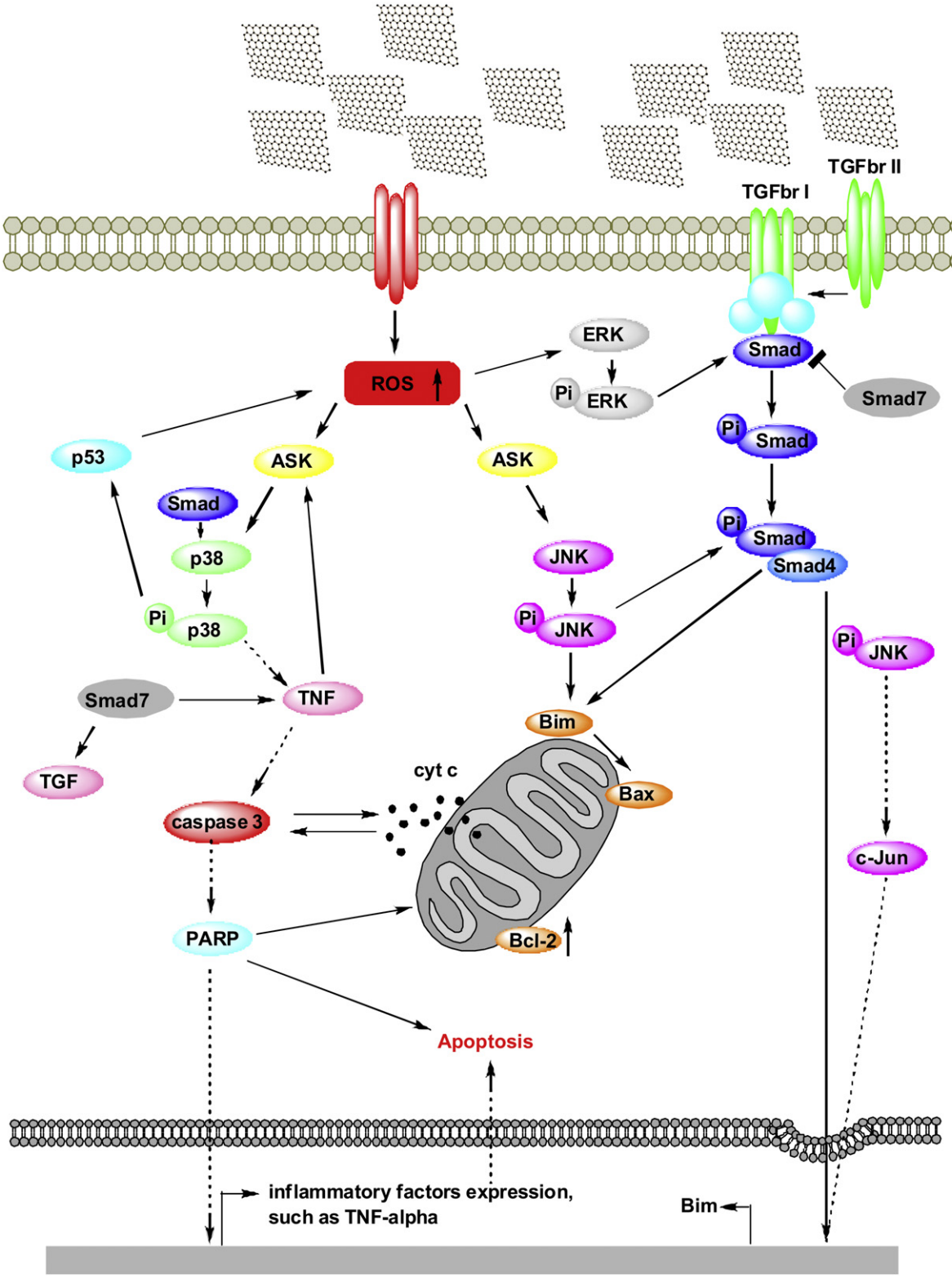

Fig. 7. Schematic diagram of signaling pathways involved in pristine graphene-induced cell apoptosis. The proposed model shows that pristine graphene causes cell apoptosis through ROS-activated MAPKs and TGF-beta pathways which regulate the mitochondria dependent apoptotic cascades.

caspase. We determined the activation of caspase-3 in pristine graphene-treated RAW 264.7 cells (Fig. 6B). The increase in the activated (cleaved) caspase-3 presented in Fig. 6B confirmed the involvement of Caspase-3 in the pristine graphene-mediated apoptosis. The involvement of caspase-3 was also confirmed by the process of PARP, a well-characterized downstream substrate of activated caspase-3 (Fig. 6B).

The chemical structure of graphene is composed of hexagonal 6-membered carbon units repeating infinitely in two dimensions and forming a thin sheet. Carbon nanotubes (CNTs) have a similar

structure. Longitudinal unzipping of a CNT and rolling-out infinitely makes graphene. Previous studies show that SWCNTs can inhibit HEK293 cells growth by inducing cell apoptosis and decreasing cellular adhesion ability associating with down-regulation of G1-assoicated cdks and cyclins and upregulation of apoptosis-associated genes [67]. Ding et al. [68] reported that interferon and p38/ERK-MAPK cascades are critical pathway components in the induced signal transduction contributing to the more adverse effects observed in human skin fibroblast cell populations exposed to multiwall carbon nano-onions (MWCNOs) and multiwall carbon nanotubes (MWCNTs). MWCNTs can activate NF-κB and AP-1 signaling pathways to induce apoptosis in rat lung epithelial cells [69]. However, many other factors would contribute to the toxicity of CNTs, like metal impurity, length, and protein binding [70–72]. The interactions of single-wall carbon nanotubes (SWCNTs) with human serum proteins demonstrated a competitive binding of these proteins with different adsorption capacity and packing modes, which can greatly alter their cellular interaction pathways and reduce the toxicity of SWCNTs [72]. The common points are that both CNTs and graphene can induce the mitochondrial damage and induce the ROS generation and further trigger the mitochondrial apoptotic pathway.

We hereby provided direct evidences that both the MAPKs- and the TGF-beta-related signaling pathways are involved in the pristine graphene-induced apoptosis in RAW 264.7 macrophages. Exposure of cells to pristine graphene can induce the loss of MMP and the accumulation of ROS. Subsequently, ROS will activate the MAPKs and TGF-beta signaling pathways, leading to the activation of Bim and Bax, which cause the permeabilization of mitochondrial outer membrane, and activates the cascade of caspases via mitochondria-related mechanisms. The activation of caspase 3 causes the execution of apoptosis finally. The summary of the mechanisms involving these signaling pathways, following pristine graphene exposure, in cell apoptosis are illustrated in a schematic diagram (Fig. 7).

4. Conclusion

In this work, the cytotoxicity and the related signaling pathways of pristine graphene in murine RAW 264.7 macrophages were evaluated. We found that the pristine graphene can induce cytotoxicity through the depletion of the mitochondrial membrane potential and the increase of intracellular reactive oxygen species, then trigger apoptosis by activation of the mitochondrial pathway. Our study demonstrates the mitochondrial pathways, the MAPKs- and TGF-beta-related signaling pathways involved in the apoptosis induced by the pristine graphene. This work provides essential information for further biomedical applications of graphene. However, better understandings for their in vivo behavior and long-term toxicology of graphene and its derivatives together with the effect of chemical modification are extremely important and further investigations are needed.

Acknowledgments

This work was financially supported by National Basic Research Program of China (973 Program, Grant Nos. 2011CB9334001 and 2010CB934004), Natural Science Foundation of China (Grant No. 10975040), CAS Knowledge Innovation Projects and National Science Council of Taiwan (Grant No. NSC 97-2113-M-002-012-MY3).

Appendix. Supplementary data

Supplementary data associated with this article can be found, in the online version, at doi:10.1016/j.biomaterials.2011.09.091.

References

[1] Zhang YB, Tan YW, Stormer HL, Kim P. Experimental observation of the quantum hall effect and Berry's phase in graphene. Nature 2005;438(7065):201–4.
[2] Liu Y, Jiao F, Qiu Y, Li W, Lao F, Zhou G, et al. The effect of Gd@C82(OH)22 nanoparticles on the release of Th1/Th2 cytokines and induction of TNF-alpha mediated cellular immunity. Biomaterials 2009;30(23–24):3934–45.
[3] Wang LM, Liu Y, Li W, Jiang XM, Ji YL, Wu XC, et al. Selective targeting of gold nanorods at the mitochondria of cancer cells: Implications for cancer therapy. Nano Lett 2011;11(2):772–80.
[4] Novoselov KS, Geim AK, Morozov SV, Jiang D, Katsnelson MI, Grigorieva IV, et al. Two-dimensional gas of massless Dirac fermions in graphene. Nature 2005;438(7065):197–200.
[5] Meyer JC, Geim AK, Katsnelson MI, Novoselov KS, Booth TJ, Roth S. The structure of suspended graphene sheets. Nature 2007;446(7131):60–3.
[6] Wu ZS, Pei SF, Ren WC, Tang DM, Gao LB, Liu BL, et al. Field emission of single-layer graphene films prepared by electrophoretic deposition. Adv Mater 2009;21(17):1756–60.
[7] Akhavan O, Abdolahad M, Esfandiar A, Mohatashamifar M. Photodegradation of graphene oxide sheets by TiO_2 nanoparticles after a photocatalytic reduction. J Phys Chem C 2010;114(30):12955–9.
[8] Bai JW, Zhong X, Jiang S, Huang Y, Duan XF. Graphene nanomesh. Nat Nanotechnol 2010;5(3):190–4.
[9] Song B, Li D, Qi WP, Elstner M, Fan CH, Fang HP. Graphene on Au(111): a highly conductive material with excellent adsorption properties for high-resolution bio/nanodetection and identification. Chem Phys Chem 2010;11(3):585–9.
[10] Sun XM, Liu Z, Welsher K, Robinson JT, Goodwin A, Zaric S, et al. Nano-graphene oxide for cellular imaging and drug delivery. Nano Res 2008;1(3):203–12.
[11] Akhavan O, Ghaderi E. Toxicity of graphene and graphene oxide nanowalls against bacteria. ACS Nano 2010;4(10):5731–6.
[12] Hu WB, Peng C, Luo WJ, Lv M, Li XM, Li D, et al. Graphene-based antibacterial paper. ACS Nano 2010;4(7):4317–23.
[13] Yang K, Zhang SA, Zhang GX, Sun XM, Lee ST, Liu ZA. Graphene in mice: ultrahigh in vivo tumor uptake and efficient photothermal therapy. Nano Lett 2010;10(9):3318–23.
[14] Zhang L, Xia J, Zhao Q, Liu L, Zhang Z. Functional graphene oxide as a nanocarrier for controlled loading and targeted delivery of mixed anticancer drugs. Small 2010;6(4):537–44.
[15] Du D, Wang LM, Shao YY, Wang J, Engelhard MH, Lin YH. Functionalized gaphene oxide as a nanocarrier in a multienzyme labeling amplification strategy for utrasensitive electrochemical immunoassay of phosphorylated p53 (S392). Anal Chem 2011;83(3):746–52.
[16] Song Y, Chen Y, Feng L, Ren J, Qu X. Selective and quantitative cancer cell detection using target-directed functionalized graphene and its synergetic peroxidase-like activity. Chem Commun; 2011:4436–8.
[17] Feng L, Chen Y, Ren J, Qu X. A graphene functionalized electrochemical aptasensor for selective label-free detection of cancer cells. Biomaterials 2011;32(11):2930–7.
[18] Gilje S, Han S, Wang M, Wang KL, Kaner RB. A chemical route to graphene for device applications. Nano Lett 2007;7(11):3394–8.
[19] Gomez-Navarro C, Weitz RT, Bittner AM, Scolari M, Mews A, Burghard M, et al. Electronic transport properties of individual chemically reduced graphene oxide sheets. Nano Lett 2007;7(11):3499–503.
[20] Schedin F, Geim AK, Morozov SV, Hill EW, Blake P, Katsnelson MI, et al. Detection of individual gas molecules adsorbed on graphene. Nat Mater 2007;6(9):652–5.
[21] Robinson JT, Perkins FK, Snow ES, Wei ZQ, Sheehan PE. Reduced graphene oxide molecular sensors. Nano Lett 2008;8(10):3137–40.
[22] Stampfer C, Schurtenberger E, Molitor F, Guttinger J, Ihn T, Ensslin K. Tunable graphene single electron transistor. Nano Lett 2008;8(8):2378–83.
[23] Standley B, Bao WZ, Zhang H, Bruck J, Lau CN, Bockrath M. Graphene-based atomic-scale switches. Nano Lett 2008;8(10):3345–9.
[24] Mohanty N, Berry V. Graphene-based single-bacterium resolution biodevice and DNA transistor: Interfacing graphene derivatives with nanoscale and microscale biocomponents. Nano Lett 2008;8(12):4469–76.
[25] Nel A, Xia T, Madler L, Li N. Toxic potential of materials at the nanolevel. Science 2006;311(5761):622–7.
[26] Shvedova AA, Kisin E, Murray AR, Johnson VJ, Gorelik O, Arepalli S, et al. Inhalation vs. aspiration of single-walled carbon nanotubes in C57BL/6 mice: inflammation, fibrosis, oxidative stress, and mutagenesis. Am J Physiol Lung Cell Mol Physiol 2008;295(4):L552–65.
[27] Wang J, Zhou G, Chen C, Yu H, Wang T, Ma Y, et al. Acute toxicity and biodistribution of different sized titanium dioxide particles in mice after oral administration. Toxicol Lett 2007;168(2):176–85.
[28] Liu YX, Li W, Lao F, Liu Y, Wang LM, Bai R, et al. Intracellular dynamics of cationic and anionic polystyrene nanoparticles without direct interaction with mitotic spindle and chromosomes. Biomaterials 2011;32:8291–303.
[29] Qu Y, Li W, Zhou YL, Liu XF, Zhang LL, Wang LM, et al. Full assessment of fate and physiological behavior of quantum dots utilizing caenorhabditis elegans as a model organism. Nano Lett 2011;11:3174–83.

[30] Ge C, Meng L, Xu L, Bai R, Du J, Zhang L, et al. Acute pulmonary and moderate cardiovascular responses of spontaneously hypertensive rats after exposure to single-wall carbon nanotubes. Nanotoxicology; 2011. doi:10.3109/17435390.2011.587905.
[31] Zhao YL, Xing GM, Chai Z. Nanotoxicology: are carbon nanotubes safe? Nat Nanotechnol 2008;3(4):191–2.
[32] Yang K, Wan J, Zhang S, Zhang Y, Lee ST, Liu Z. In vivo pharmacokinetics, long-term biodistribution, and toxicology of PEGylated graphene in mice. ACS Nano; 2010:1840–54.
[33] Chang Y, Yang ST, Liu JH, Dong E, Wang Y, Cao A, et al. In vitro toxicity evaluation of graphene oxide on A549 cells. Toxicol Lett; 2010:201–10.
[34] Zhang Y, Ali SF, Dervishi E, Xu Y, Li Z, Casciano D, et al. Cytotoxicity effects of graphene and single-wall carbon nanotubes in neural phaeochromocytoma-derived PC12 cells. ACS Nano; 2010:706–10.
[35] Wang K, Ruan J, Song H, Zhang J, Wo Y, Guo S, et al. Biocompatibility of graphene oxide. Nanoscale Res Lett; 2010:1–8.
[36] Thubagere A, Reinhard BM. Nanoparticle-induced apoptosis propagates through hydrogen-peroxide-mediated bystander killing: insights from a human intestinal epithelium in vitro model. ACS Nano 2010;4(7):3611–22.
[37] Fahmy B, Cormier SA. Copper oxide nanoparticles induce oxidative stress and cytotoxicity in airway epithelial cells. Toxicol In Vitro 2009;23(7):1365–71.
[38] Gurr JR, Wang ASS, Chen CH, Jan KY. Ultrafine titanium dioxide particles in the absence of photoactivation can induce oxidative damage to human bronchial epithelial cells. Toxicology 2005;213(1–2):66–73.
[39] Nakagawa H, Hasumi K, Woo JT, Nagai K, Wachi M. Generation of hydrogen peroxide primarily contributes to the induction of Fe(II)-dependent apoptosis in Jurkat cells by (-)-epigallocatechin gallate. Carcinogenesis 2004;25(9):1567–74.
[40] Qiu Y, Liu Y, Wang L, Xu L, Bai R, Ji Y, et al. Surface chemistry and aspect ratio mediated cellular uptake of Au nanorods. Biomaterials 2010;31:7606–19.
[41] Chipuk J, Bouchier-Hayes L, Green D. Mitochondrial outer membrane permeabilization during apoptosis: the innocent bystander scenario. Cell Death Differ 2006;13(8):1396–402.
[42] Kroemer G, Galluzzi L, Brenner C. Mitochondrial membrane permeabilization in cell death. Physiol Rev 2007;87(1):99–163.
[43] Hengartner MO. The biochemistry of apoptosis. Nature 2000;407(6805):770–6.
[44] Lao F, Chen L, Li W, Ge C, Qu Y, Sun Q, et al. Fullerene nanoparticles selectively enter oxidation-damaged cerebral microvessel endothelial cells and inhibit JNK-related apoptosis. ACS Nano 2009;3(11):3358–68.
[45] Davis RJ. Signal transduction by the JNK group of MAP kinases. Cell 2000;103(2):239–52.
[46] Cuda G, Paterno R, Ceravolo R, Candigliota M, Perrotti N, Perticone F, et al. Protection of human endothelial cells from oxidative stress - role of Ras-ERK1/2 signaling. Circulation 2002;105(8):968–74.
[47] Johnson NL, Gardner AM, Diener KM, LangeCarter CA, Gleavy J, Jarpe MB, et al. Signal transduction pathways regulated by mitogen-activated extracellular response kinase kinase kinase induce cell death. J Biol Chem 1996;271(6):3229–37.
[48] Moreno-Manzano V, Ishikawa Y, Lucio-Cazana J, Kitamura M. Suppression of apoptosis by all-trans-retinoic acid - Dual intervention in the c-Jun N-terminal kinase-AP-1 pathway. J Biol Chem 1999;274(29):20251–8.
[49] Pan JS, Hong MZ, Ren JL. Reactive oxygen species: a double-edged sword in oncogenesis. World J Gastroentero 2009;15(14):1702–7.
[50] Ray G, Dhar G, Van Veldhuizen PJ, Banerjee S, Saxena NK, Sengupta K, et al. Modulation of cell-cycle regulatory signaling network by 2-methoxyestradiol in prostate cancer cells is mediated through multiple signal transduction pathways. Biochemistry (Mosc) 2006;45(11):3703–13.
[51] Cho SD, Li GX, Hu HB, Jiang C, Kang KS, Lee YS, et al. Involvement of c-Jun N-terminal kinase in G(2)/M arrest and caspase-mediated apoptosis induced by sulforaphane in DU145 prostate cancer cells. Nutr Cancer 2005;52(2):213–24.
[52] Miyoshi N, Uchida K, Osawa T, Nakamura Y. Benzyl isothiocyanate modifies expression of the G(2)/M arrest-related genes. Biofactors 2004;21(1–4):23–6.
[53] Shi Y, Sahu RP, Srivastava SK. Triphala inhibits both in vitro and in vivo xenograft growth of pancreatic tumor cells by inducing apoptosis. BMC Cancer 2008;8:294–316.
[54] Kim MH, Kim MO, Heo JS, Kim JS, Han HJ. Acetylcholine inhibits long-term hypoxia-induced apoptosis by suppressing the oxidative stress-mediated MAPKs activation as well as regulation of Bcl-2, c-IAPs, and caspase-3 in mouse embryonic stem cells. Apoptosis 2008;13(2):295–304.
[55] Kuo PL, Chen CY, Hsu YL. Isoobtusilactone A induces cell cycle arrest and apoptosis through reactive oxygen species/apoptosis signal-regulating kinase 1 signaling pathway in human breast cancer cells. Cancer Res 2007;67(15):7406–20.
[56] Noguchi T, Ishii K, Fukutomi H, Naguro I, Matsuzawa A, Takeda K, et al. Requirement of reactive oxygen species-dependent activation of ASK1-p38 MAPK pathway for extracellular ATP-induced apoptosis in macrophage. J Biol Chem 2008;283(12):7657–65.
[57] Lomo J, Blomhoff HK, Beiske K, Stokke T, Smeland EB. TGF-beta-1 and cyclic-AMP promote apoptosis in resting human B-lymphocytes. J Immunol 1995;154(4):1634–43.
[58] Chaouchi N, Arvanitakis L, Auffredou MT, Blanchard DA, Vazquez A, Sharma S. Characterization of transforming growth-factor-beta-1 induced apoptosis in normal human B-cells and lymphoma B-cell lines. Oncogene 1995;11(8):1615–22.
[59] Patil S, Wildey GM, Brown TL, Choy L, Derynck R, Howe PH. Smad7 is induced by CD40 and protects WEHI 231 B-lymphocytes from transforming growth factor-beta-induced growth inhibition and apoptosis. J Biol Chem 2000;275(49):38363–70.
[60] Lallemand F, Mazars A, Prunier C, Bertrand F, Kornprost M, Gallea S, et al. Smad7 inhibits the survival nuclear factor kappa B and potentiates apoptosis in epithelial cells. Oncogene 2001;20(7):879–84.
[61] Leivonen SK, Hakkinen L, Liu D, Kahari VM. Smad3 and extracellular signal-regulated kinase 1/2 coordinately mediate transforming growth factor-beta-induced expression of connective tissue growth factor in human fibroblasts. J Invest Dermatol 2005;124(6):1162–9.
[62] Schuster N, Krieglstein K. Mechanisms of TGF-beta-mediated apoptosis. Cell Tissue Res 2002;307(1):1–14.
[63] Ramesh S, Wildey GM, Howe PH. Transforming growth factor beta (TGF beta)-induced apoptosis the rise & fall of bim. Cell Cycle 2009;8(1):11–7.
[64] Ghavami S, Hashemi M, Ande SR, Yeganeh B, Xiao W, Eshraghi M, et al. Apoptosis and cancer: mutations within caspase genes. J Med Genet 2009;46(8):497–510.
[65] Salvesen GS. Caspases: opening the boxes and interpreting the arrows. Cell Death Differ 2002;9(1):3–5.
[66] Yu SW, Wang HM, Poitras MF, Coombs C, Bowers WJ, Federoff HJ, et al. Mediation of poly(ADP-ribose) polymerase-1-dependent cell death by apoptosis-inducing factor. Science 2002;297(5579):259–63.
[67] Cui D, Tian F, Ozkan CS, Wang M, Gao H. Effect of single wall carbon nanotubes on human HEK293 cells. Toxicol Lett 2005;155:73–85.
[68] Ding LH, Stilwell J, Zhang TT, Elboudwarej O, Jiang H, Selegue JP, et al. Molecular characterization of the cytotoxic mechanism of multiwall carbon nanotubes and nanoonions on human skin fibroblast. Nano Lett 2005;5(12):2448–64.
[69] Ravichandran P, Baluchamy S, Sadanandan B, Gopikrishnan R, Biradar S, Ramesh V, et al. Multiwalled carbon nanotubes activate NF-κB and AP-1 signaling pathways to induce apoptosis in rat lung epithelial cells. Apoptosis 2010;15:1507–16.
[70] Ge C, Lao F, Li W, Li Y, Chen C, Qiu Y, et al. Quantitative analysis of metal impurities in carbon nanotubes: Efficacy of different pretreatment protocols for ICPMS spectroscopy. Anal Chem 2008;80(24):9426–34.
[71] Ge C, Li W, Li Y, Lao F, Qiu Y, Liu Y, et al. Significance and systematic analysis of metallic impurities of carbon nanotubes produced by different manufacturers. J Nanoscience Nanotechnol 2011;11:2389–97.
[72] Ge C, Du J, Zhao L, Wang L, Liu Y, et al. Binding of blood proteins to carbon nanotubes reduces cytoxicity. PNAS; 2011. doi:10.1073/pnas.1105270108.